Diffusion Tensor Imaging of Visual Pathway Abnormalities in Five Glaucoma Animal Models

Max K. Colbert,[1] Leon C. Ho,[2] Yolandi van der Merwe,[2] Xiaoling Yang,[2] Gillian J. McLellan,[3,4] Samuel A. Hurley,[5] Aaron S. Field,[5] Hongmin Yun,[2] Yiqin Du,[2] Ian P. Conner,[2] Carlos Parra,[1] Muneeb A. Faiq,[1] John H. Fingert,[6] Gadi Wollstein,[1,7,8] Joel S. Schuman,[1,7–9] and Kevin C. Chan[1,7–10]

[1]Department of Ophthalmology, NYU Grossman School of Medicine, NYU Langone Health, New York University, New York, New York, United States
[2]Department of Ophthalmology, University of Pittsburgh School of Medicine, Pittsburgh, Pennsylvania, United States
[3]Department of Ophthalmology and Visual Sciences, University of Wisconsin - Madison, Madison, Wisconsin, United States
[4]McPherson Eye Research Institute, University of Wisconsin - Madison, Madison, Wisconsin, United States
[5]Department of Radiology, University of Wisconsin - Madison, Madison, Wisconsin, United States
[6]Department of Ophthalmology and Visual Sciences, University of Iowa College of Medicine, Iowa City, Iowa, United States
[7]Center for Neural Science, College of Arts and Science, New York University, New York, New York, United States
[8]Department of Biomedical Engineering, New York University Tandon School of Engineering, Brooklyn, New York, United States
[9]Neuroscience Institute, NYU Grossman School of Medicine, NYU Langone Health, New York University, New York, New York, United States
[10]Department of Radiology, NYU Grossman School of Medicine, NYU Langone Health, New York University, New York, New York, United States

Correspondence: Kevin C. Chan, 222 E 41st Street, Room 362, Departments of Ophthalmology and Radiology, NYU Grossman School of Medicine, NYU Langone Health, New York University, New York, NY 10017, USA; chuenwing.chan@fulbrightmail.org.

MKC and LCH contributed equally to this work.

Received: January 11, 2021
Accepted: July 26, 2021
Published: August 19, 2021

Citation: Colbert MK, Ho LC, van der Merwe Y, et al. Diffusion tensor imaging of visual pathway abnormalities in five glaucoma animal models. *Invest Ophthalmol Vis Sci.* 2021;62(10):21. https://doi.org/10.1167/iovs.62.10.21

Purpose. To characterize the visual pathway integrity of five glaucoma animal models using diffusion tensor imaging (DTI).

Methods. Two experimentally induced and three genetically determined models of glaucoma were evaluated. For inducible models, chronic IOP elevation was achieved via intracameral injection of microbeads or laser photocoagulation of the trabecular meshwork in adult rodent eyes. For genetic models, the DBA/2J mouse model of pigmentary glaucoma, the *LTBP2* mutant feline model of congenital glaucoma, and the transgenic *TBK1* mouse model of normotensive glaucoma were compared with their respective genetically matched healthy controls. DTI parameters, including fractional anisotropy, axial diffusivity, and radial diffusivity, were evaluated along the optic nerve and optic tract.

Results. Significantly elevated IOP relative to controls was observed in each animal model except for the transgenic *TBK1* mice. Significantly lower fractional anisotropy and higher radial diffusivity were observed along the visual pathways of the microbead- and laser-induced rodent models, the DBA/2J mice, and the *LTBP2*-mutant cats compared with their respective healthy controls. The DBA/2J mice also exhibited lower axial diffusivity, which was not observed in the other models examined. No apparent DTI change was observed in the transgenic *TBK1* mice compared with controls.

Conclusions. Chronic IOP elevation was accompanied by decreased fractional anisotropy and increased radial diffusivity along the optic nerve or optic tract, suggestive of disrupted microstructural integrity in both inducible and genetic glaucoma animal models. The effects on axial diffusivity differed between models, indicating that this DTI metric may represent different aspects of pathological changes over time and with severity.

Keywords: diffusion tensor imaging, glaucoma, intraocular pressure, magnetic resonance imaging, optic neuropathy, visual pathway

Glaucoma is a neurodegenerative disease marked by progressive vision loss in association with injuries to the retinal ganglion cells (RGCs) and their axons in the optic nerve. It is the leading cause of irreversible blindness in the world, affecting more than 79 million people worldwide,[1–3] and will become even more prevalent in the years to come as a byproduct of increased longevity in an aging population. An elevated IOP is considered a major risk factor for glaucoma. However, the relationship between IOP and disease phenotype is complex. For example, tonometric screening

for IOP has a sensitivity and positive predictive value of 80.1% and 52.1% for glaucoma, respectively. Additionally, approximately 20% of subjects with glaucoma have normal IOP, whereas nearly 90% of subjects with elevated IOP do not go on to develop the disease.[4–6] Furthermore, glaucomatous neurodegeneration may proceed even after IOP has been controlled via medical or surgical interventions.[5] These findings indicate that the overall mechanisms underlying the development of glaucoma are not fully understood.

Recent studies in humans and animal models suggest extensive involvement of the brain's visual system in glaucoma, from inner retinal thinning and distal optic axonopathy, to neuronal cell loss in the lateral geniculate nucleus, trans-synaptic neurodegeneration of the optic radiation, and metabolic or functional modulation in the visual cortex.[7–14] However, its extent across different etiopathogeneses remains poorly defined, partly owing to limited *in vivo* studies to monitor the spatiotemporal changes occurring along the visual pathway in response to the disease.[15,16] Diffusion tensor imaging (DTI) is a noninvasive magnetic resonance imaging (MRI) technique that exploits the anisotropic water diffusion in the white matter tracts to estimate the organization of the brain. Among the DTI-derived parameters, fractional anisotropy (FA) describes the directionality of white matter tracts and is an imaging biomarker for the overall microstructural integrity of the brain, whereas the directional diffusivities, including axial diffusivity ($\lambda_{//}$) and radial diffusivity ($\lambda_{\perp}$) describe the magnitude of diffusion parallel and perpendicular to the fiber tracts, respectively, and may reflect more specific pathophysiological changes such as axonal and myelin integrity.[17–20] DTI has been used for evaluating the microstructural environment in various neurodegenerative processes, including human glaucoma with mixed results. To date, the use of DTI in characterizing chronic experimental glaucoma remains sparse.

In this study, we used DTI to evaluate the white matter integrity along the optic nerve and optic tract in two experimentally induced models and three genetically determined models of glaucoma. For inducible glaucoma animal models, we used two common procedures involving the intracameral injection of microbeads and laser photocoagulation of the trabecular meshwork, both of which require a relatively short span of time to develop a glaucomatous phenotype. For genetic animal models, Dilute Brown Non-Agouti (DBA/2J) mice and latent-transforming growth factor beta-binding protein 2 (*LTBP2*) mutant cats are characterized by spontaneous IOP elevation and RGC loss,[21,22] and were selected as IOP-dependent glaucoma animal models, whereas TANK-binding kinase 1 (*TBK1*) duplications have been implicated as a risk factor for the development of normal tension glaucoma in humans, and its hemizygous transgenic mouse model was included in this study to evaluate for any potential microstructural aberrations.[23] We hypothesize that specific induction of pathogenic processes associated with different glaucoma models may alter the diffusion indices along the optic nerve and optic tract owing to their specific damage to the microstructural environment.

Methods

All procedures were carried out in accordance with the ARVO Statement for the Use of Animals in Ophthalmic and Vision Research. The rodent and feline studies were performed with the approval of the appropriate Institutional Animal Care and Use Committees at the University of Pittsburgh, the University of Wisconsin-Madison, and the University of Iowa.

Animal Preparation

Microbead-induced Experimental Glaucoma. Eight adult Sprague-Dawley rats received an injection of a mixture of 5 µL of 10 µm microbeads and 5 µL of 15 µm microbeads into the anterior chamber of the right eye to block aqueous outflow and induce sustained elevation of IOP for about 4 weeks. The left eye was untreated and served as an internal control. An MRI was performed at 4 weeks after injection, because prior findings suggest that this duration may approximate the upper limit of sustainable IOP elevation achievable from a single injection procedure with a 20% loss in axons at about 4 weeks.[24,25]

Laser-induced Experimental Glaucoma. The IOP of seven adult C57BL/6J mice was increased by disrupting aqueous outflow in both eyes using 532-nm green laser photocoagulation to the trabecular meshwork.[21] Six age-matched healthy C57BL/6J mice were left untreated and served as controls. Prior studies have analyzed the IOP-elevating capability of a single laser photocoagulation procedure up to 6 months, with a 59% decrease in axon density in optic nerves associated with significant reduction in RGCs.[21] For this reason, MRI was performed at 8 months after laser treatment to further characterize the long-term potential of laser photocoagulation models for studying the relationship between elevated IOP and microstructural integrity in the visual pathway.

Genetic Glaucoma Animal Models. Three genetically determined glaucoma animal models and their controls were used: (1) The DBA/2J mouse model of hereditary pigmentary glaucoma[26] ($n = 8$) and its genetically matched DBA/2J-Gpnmb^{+} control strain ($n = 8$) were imaged longitudinally at 7, 9, and 12 months of age. These time points were selected to reflect the known spontaneous IOP increase in DBA/2J mice at approximately 8 to 9 months and the severe optic nerve damage present at around 12 months of age[27] along with about 44% RGC loss.[28,29] (2) The feline (*Felis catus*) model of primary congenital glaucoma homozygous for mutation in *LTBP2*[22] ($n = 3$) and age-matched normal wild-type domestic short-hair cats ($n = 3$) were scanned at 4 to 8 years of age to demonstrate if glaucomatous damage can be detected noninvasively using DTI in this established and long-lived disease model. *LTBP2* cats are documented to exhibit up to 64% RGC loss across this range of timepoints.[22] (3) The transgenic hemizygous *TBK1* mouse model of normal tension glaucoma[23] ($n = 4$) and its wild-type littermates ($n = 4$) were scanned at about 20 months of age, a late time point selected to expand on prior work evaluating the characteristics of this model up to 18 months, where hemizygous *TBK1* mice exhibited a 13% RGC loss.[23] All control animals were free of the *rd1* mutation responsible for retinal degeneration.

Tonometry

The IOP values for the microbead, laser, DBA/2J, and *TBK1* models were measured using a handheld TonoLab rebound tonometer (Icare Finland Oy, Vantaa, Finland) within 5 minutes after isoflurane gas anesthesia induction, whereas IOP measurements in cats were acquired using

TonoVet rebound tonometry (Icare Finland Oy) without sedation. This procedure was repeated to obtain at least three instrument-derived IOP values for each eye, and the average value was used for final analysis.

MRI Protocol

Rodents were anesthetized with a mixture of air and isoflurane (3.0% for induction and 1.5% for maintenance) during MRI experiments with respiratory rate monitoring. Rodent DTI was acquired using a 9.4-Tesla/31-cm Varian/Agilent horizontal bore scanner with a 32 mm transmit–receive volume coil using a fast spin-echo sequence, with 12 diffusion gradient directions at diffusion-weighting factor (b) = 1000 s/mm^2 and two additional b_o images at b = 0 s/mm^2. Other imaging parameters included a repetition time/echo time of 2300/27.8 ms, an echo train length of 8, number of averages of 4, field of view of 2.6 × 2.6 cm^2 (rats) and 2 × 2 cm^2 (mice), acquisition matrix of 192 × 192 (zero-filled to 256 × 256), and slice thickness of 0.5 mm. Slices were oriented orthogonal to the prechiasmatic optic nerves.

Cats were anesthetized by intramuscular injection of ketamine (12.5–25.0 mg/kg) and xylazine (0.5–2.0 mg/kg). Heart rate and oxygenation were monitored by pulse oximetry throughout the MRI procedure. Cat DTI was performed on a 3-Tesla GE Discovery MR750 scanner with a GEM Flex Medium coil, using a spin-echo sequence, with 40 diffusion gradient directions at a b value of 1300 s/mm^2 and eight non–diffusion-weighted b_o images at a b value of 0 s/mm^2. Other imaging parameters included a repetition time/echo time of 8000/96.2 ms, number of averages of 1, a field of view of 10 × 10 cm^2, an acquisition matrix of 96 × 96, and a slice thickness of 2.9 mm.

Data Analysis

Coregistration between b_o and diffusion-weighted images were performed using SPM8 (Wellcome Department of Imaging Neuroscience, University College, London, UK). DTI parameter maps including FA, $\lambda_{//}$, and $\lambda_{\perp}$ maps were computed using DTIStudio v3.02 (Johns Hopkins University, Baltimore, MD). Manual regions of interest were drawn on the optic nerves and optic tracts using ImageJ v1.47 (Rasband, W.S., National Institutes of Health, Bethesda, MD, USA) based on FA maps and then applied to the $\lambda_{//}$ and $\lambda_{\perp}$ maps. The region of interest selection was conducted with blinding by our investigators without knowing which groups or eyes were experimental and which ones were control until statistical analyses were to be performed. For the feline model, only the optic tracts and the nearby internal capsules were measured because of distortion artifacts at the level of the optic nerve as well as partial volume effects from limited resolution at 3 Tesla relative to the size of the optic nerve. DTI parametric values from the DBA/2J model were compared between groups and across age using ANOVA and post hoc Sidak multiple comparisons correction tests by GraphPad Prism v6.00 (GraphPad Software Inc., La Jolla, CA), whereas the other animal models were compared using two-tailed paired *t* tests within experimental groups or two-tailed unpaired *t* tests between experimental and control groups using GraphPad Prism. Data are represented as mean ± standard error of the mean. Results were considered statistically significant when the *P* is less than 0.05.

Results

IOP

The demographics and IOP values of each group are summarized in Table. In brief, the treated eyes of the microbead-induced and laser-induced rodent models and the eyes of *LTBP2* mutant cats demonstrated significantly higher IOPs than their respective controls at the imaging time points. Significant IOP elevation was also observed in the DBA/2J mice at 9 and 12 months old but not at 7 months old. No apparent IOP difference was observed between the transgenic *TBK1* mice and their age-matched controls.

DTI Abnormalities in the Inducible Glaucoma Animal Models

In the rat model of microbead-induced experimental glaucoma (Fig. 1), the optic nerve ipsilateral to the microbead-injected right eye exhibited significantly lower FA compared with that projected from the untreated left eye. Comparisons of directional diffusivities in these animals revealed a significantly higher $\lambda_{\perp}$ in the right optic nerves relative to the left optic nerves. No apparent difference in $\lambda_{//}$ was observed between left and right optic nerves. There was no statistically significant difference in DTI parameters between the left and right optic tracts in this model.

Analyses of FA, $\lambda_{//}$, and $\lambda_{\perp}$ in the mouse model of laser-induced experimental glaucoma yielded similar results (Fig. 2). Mice subjected to chronic IOP elevation displayed significantly lower FA and higher $\lambda_{\perp}$ in the optic nerve compared with their age-matched controls without a change in the $\lambda_{//}$. No significant difference in FA, $\lambda_{//}$, or $\lambda_{\perp}$ was observed along the optic tracts between experimental and control groups.

Table. Demographics and IOP Values in Each of the Experimental and Control Groups

				Glaucoma		Healthy Control		
Model	**Species**	**Strain**	**Imaging Time Point**	**IOP (mm Hg)**	***n***	**IOP (mm Hg)**	***n***	**Sig.**
Microbead	Rat	Sprague-Dawley	1 month after induction	27.28 ± 3.01	8	14.36 ± 0.66	8	**
Laser	Mouse	C57BL/6J	8 months after induction	28.14 ± 2.49	7	14.23 ± 2.65	6	**
DBA/2J	Mouse	DBA/2J or DBA/2J-Gpnmb$^+$	7 months old	14.73 ± 1.40	8	11.51 ± 0.31	8	n.s.
			9 months old	19.66 ± 1.48	8	9.87 ± 0.41	8	**
			12 months old	25.19 ± 1.43	8	10.76 ± 0.40	8	***
LTBP2	Cat	Domestic short-hair (*F catus*)	4–8 years old	57.83 ± 8.33	3	16.56 ± 2.33	3	***
TBK1	Mouse	C57BL/6J	20 months old	15.91 ± 1.18	4	15.72 ± 1.42	4	n.s.

Data are represented as mean ± standard error of the mean. Sig: Significance; *t* test between glaucoma and healthy control groups: *P < 0.05; **P < 0.01; ***P < 0.001; n.s. = not significant.

Investigative Ophthalmology & Visual Science

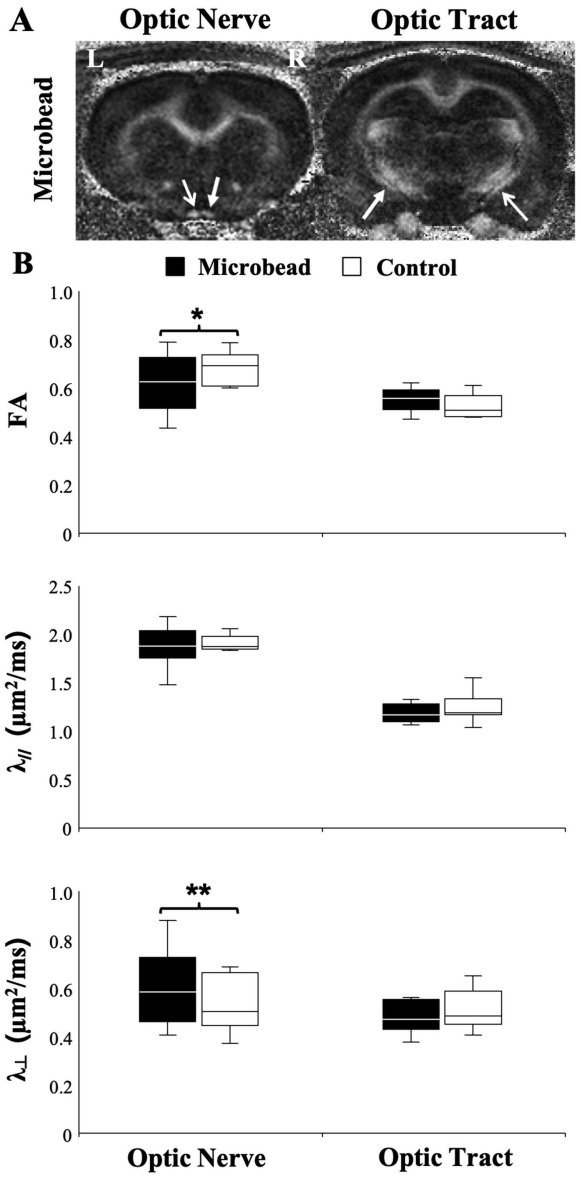

Figure 1. DTI of the rat optic nerve and optic tract under microbead-induced experimental glaucoma versus control. (**A**) FA maps showing the injured right optic nerve and left optic tract (*closed arrows*) after experimental glaucoma induction in the right eye via intracameral microbead injection, and the left optic nerve and right optic tract corresponding with the untreated control left eye (*open arrows*). (**B**) Comparisons of FA, axial diffusivity ($\lambda_{//}$), and radial diffusivity ($\lambda_{\perp}$) between the optic nerves and tracts projected from the glaucomatous right eyes (*black*) and the control left eyes (*white*). A *t* test between glaucomatous and control visual pathways: $^{*}P < 0.05$; $^{**}P < 0.01$. Data are displayed as box and whisker plots, with caps representing minimum and maximum values, and boxes representing interquartile range with median line shown.

DTI Abnormalities in the Genetic Glaucoma Animal Models

Quantitative comparisons between DBA/2J mice and their genetically matched DBA/2J-Gpnmb^{+} controls demonstrated significantly lower FA, higher $\lambda_{\perp}$, and lower $\lambda_{//}$ in the optic nerves of the DBA/2J mice at 12 months old (Fig. 3). In the optic tracts of the DBA/2J mice, significantly lower FA and higher $\lambda_{\perp}$ were also observed in the DBA/2J mice

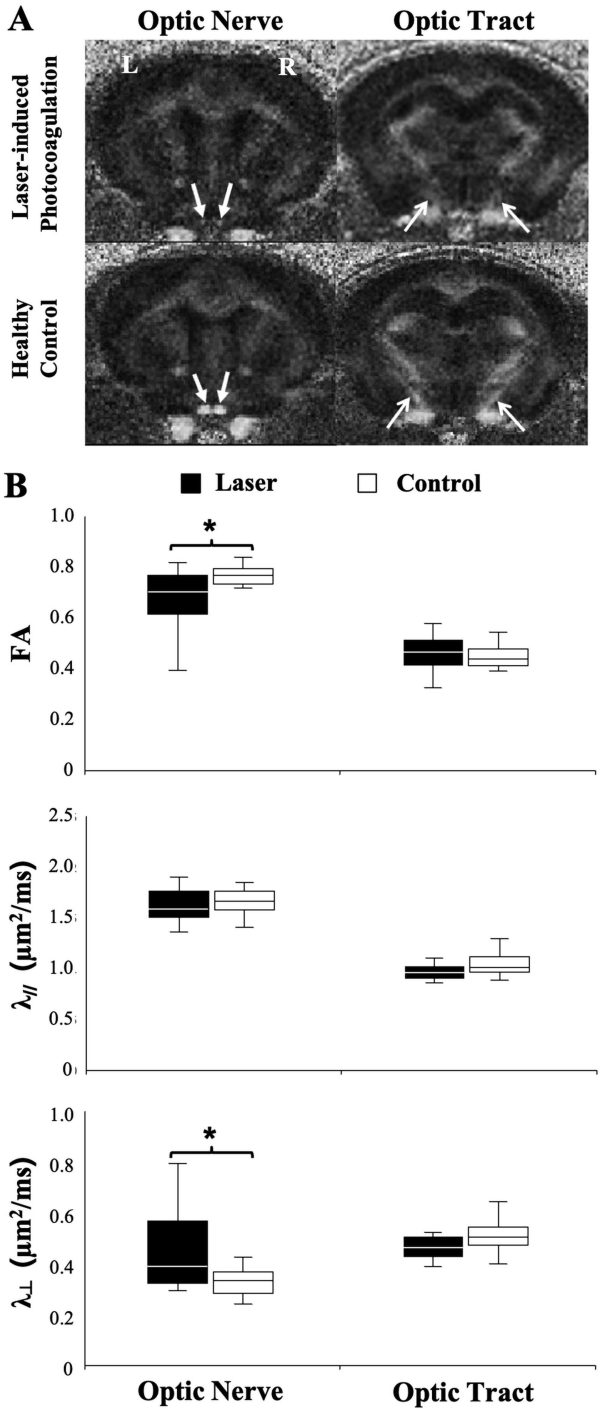

Figure 2. DTI of the mouse optic nerve and optic tract under laser-induced experimental glaucoma versus age-matched controls. (**A**) FA maps showing the optic nerves (*closed arrows*) and optic tracts (*open arrows*) after experimental glaucoma induction via bilateral laser photocoagulation of the mouse trabecular meshwork (*top row*), and in the healthy control mice (*bottom row*). (**B**) Comparisons of FA, axial diffusivity ($\lambda_{//}$), and radial diffusivity ($\lambda_{\perp}$), between glaucomatous (*black*) and control visual pathways (*white*). A *t* test between glaucoma and control mice: $^{*}P < 0.05$. Data are displayed as box and whisker plots, with caps representing minimum and maximum values, and boxes representing interquartile range with median line shown.

Investigative Ophthalmology & Visual Science

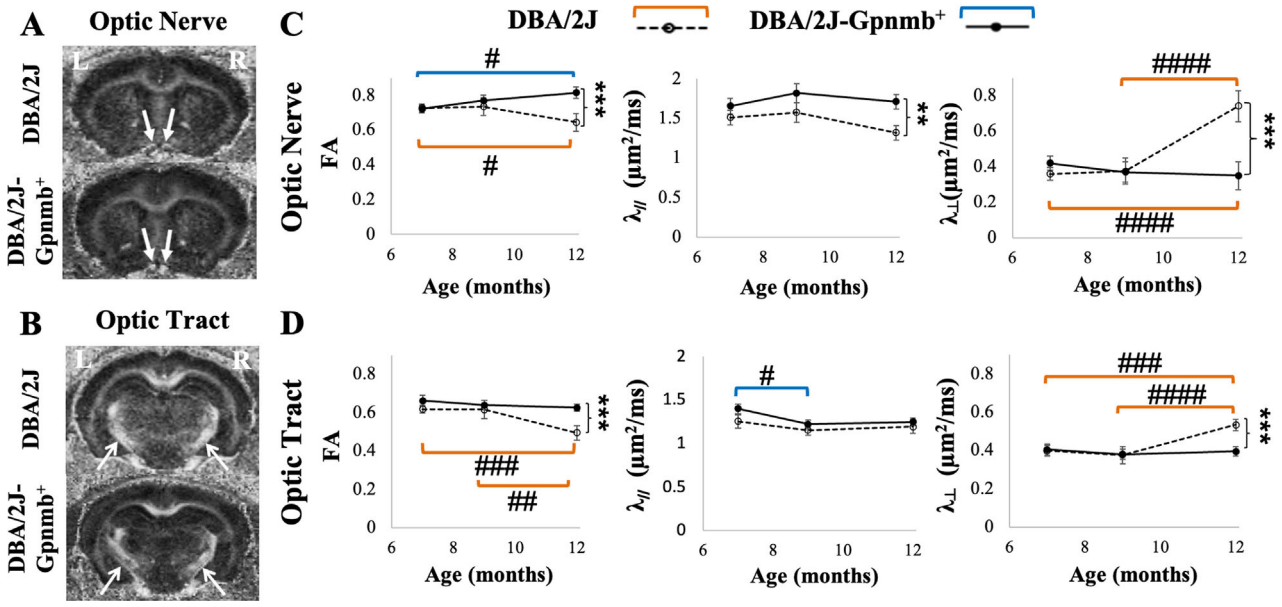

Figure 3. Longitudinal analysis of DTI parameters in the DBA/2J mouse model of pigmentary glaucoma and the DBA/2J-Gpnmb$^+$ control strain. (**A**, **B**) FA maps showing the optic nerves (**A**, *closed arrows*) and optic tracts (**B**, *open arrows*) of the DBA/2J (*top*) and DBA/2J-Gpnmb$^+$ control groups (*bottom*) at 12 months old. (**C**, **D**) Comparisons of FA, axial diffusivity ($\lambda_{//}$), and radial diffusivity ($\lambda_\perp$) in the optic nerves (**C**) and optic tracts (**D**) between DBA/2J and DBA/2J-Gpnmb$^+$ groups at 7, 9, and 12 months old. Post hoc Sidak tests between DBA/2J and DBA/2J-Gpnmb$^+$ mice: $^*P < 0.05$, $^{**}P < 0.01$, $^{***}P < 0.001$; between ages within the same strains: $^{\#}P < 0.05$, $^{\#\#}P < 0.01$, $^{\#\#\#}P < 0.001$, $^{\#\#\#\#}P < 0.0001$, with *orange and blue brackets* indicating longitudinal comparisons within DBA/2J and DBA/2J-Gpnmb$^+$ groups, respectively. Data are represented as mean ± standard error of the mean.

relative to the controls at 12 months old in a smaller extent as compared with the optic nerve.

In the *LTBP2* mutant feline model of glaucoma, significantly lower FA and higher $\lambda_\perp$ were observed in the optic tracts of the *LTBP2* mutant cats compared with healthy controls (Fig. 4), whereas no apparent difference in $\lambda_{//}$ was identified in the optic tracts. No DTI difference was observed in the internal capsule between the glaucomatous and control groups in the feline model. Quantitative comparisons of FA, $\lambda_{//}$, and $\lambda_\perp$ between transgenic *TBK1* mice and wild-type littermates revealed no apparent difference in either the optic nerve or optic tract (Fig. 5).

Discussion

The results of the present study demonstrate that the glaucoma rodent models used, with the exception of the transgenic *TBK1* mice, consistently exhibited lower FA and higher $\lambda_\perp$ in the intracranial optic nerve relative to their respective controls. Lower FA and higher $\lambda_\perp$ were also observed in the postchiasmatic optic tract of the DBA/2J mice and the *LTBP2* mutant cats. Among these models, only the DBA/2J mice showed lower $\lambda_{//}$ at the level of the optic nerve. To date, the majority of human glaucoma DTI studies have focused on FA decrease in the visual pathways in patients with glaucoma,[30–36] which could be detected before substantial clinical vision loss occurred.[37] Several studies have also examined the specific directional diffusivities along the visual pathways in patients with glaucoma, but the results have been mixed, with studies variously reporting $\lambda_{//}$ increase,[38–41] $\lambda_{//}$ decrease,[37] or no $\lambda_{//}$ change,[42–44] and some showing $\lambda_\perp$ increase[37,38,40,41,43,44] or $\lambda_\perp$ decrease.[42] These disparate results in humans suggest that different etiologies, stages, or severities of human glaucoma may yield varying neurologic manifestations. Thus, a broad, well-defined set of glaucoma animal models of diverse species and etiopathogeneses may reflect distinct aspects of glaucoma for understanding the neurologic impacts of the disease and therapeutic responses. The present study contributes to this effort using noninvasive DTI to characterize the microstructural profiles along the optic nerve and optic tract of commonly used animal models of glaucoma. These findings can be essential to guide model selection when designing future studies requiring the noninvasive monitoring of neurologic response to disease and treatment.

In the present study, chronic IOP elevation in both inducible and genetic models of glaucoma was accompanied by decreased FA, indicative of aberrant microstructural integrity along the visual pathway in these models detectable with DTI.[22,25,26,28,45] As for directional diffusivities, the $\lambda_\perp$ increase observed in our experimental models concurs with most human glaucoma DTI studies, suggestive of pathophysiological events that can increase water diffusion perpendicular to the RGC axon projections, such as demyelination, inflammation, and glial activation.[40,46–51] The DBA/2J mouse model of pigmentary glaucoma was the only model in this study to demonstrate decreased $\lambda_{//}$ at the level of the optic nerve along with a $\lambda_\perp$ increase. We speculate that such a decrease in the $\lambda_{//}$ may be a result of axonal degeneration and astrocyte reorganization,[52,53] whereas the lack of differences in $\lambda_{//}$ in other models may be attributed to a combination of axonal injury (which may decrease $\lambda_{//}$), neuroinflammation (which may increase or decrease $\lambda_{//}$),[28,47,48] and axonal loss (which may increase $\lambda_{//}$ in chronic and slow progressing white matter degeneration).[54] It is also possible that the time to reach maximal damage is different between models and, therefore, it might take more time for a particular model to reach the same point

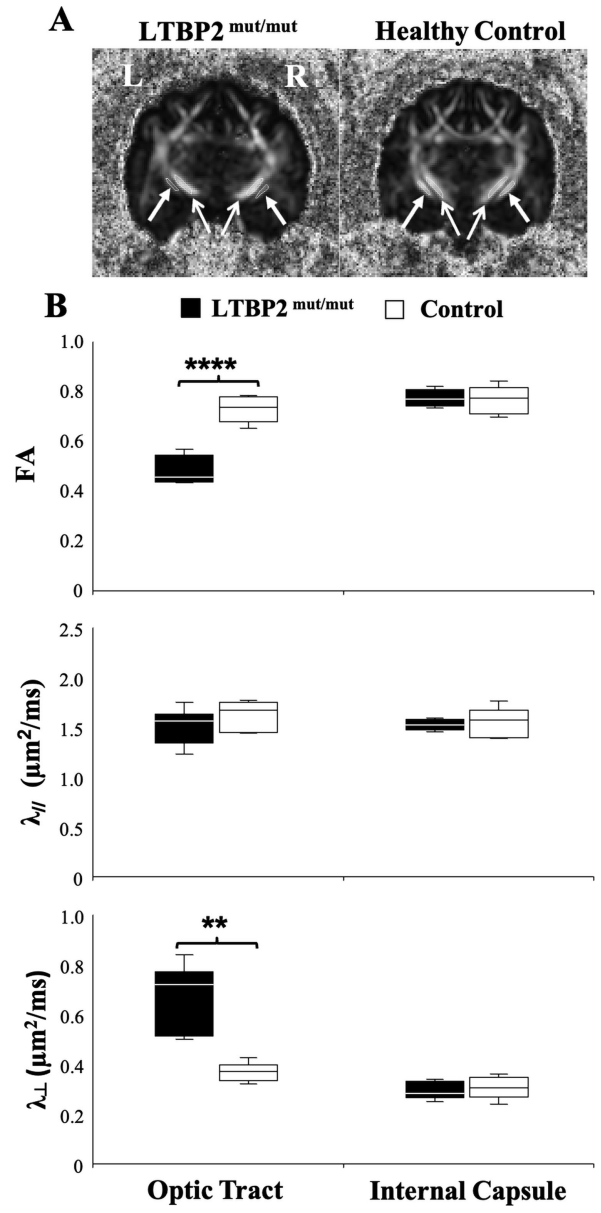

Figure 4. DTI of the feline model of congenital glaucoma owing to homozygous *LTBP2* mutation. (**A**) FA maps at the level of the optic tracts (*closed arrows*) and internal capsules (*open arrows*) in the *LTBP2*$^{mut/mut}$ cats (*left*) and healthy controls (*right*). The internal capsules served as an internal control to determine whether any observed differences in the optic tracts of glaucomatous and control cats were specific to the visual pathway or reflected more generalized neuropathology. (**B**) Comparisons of FA, axial diffusivity ($\lambda_{//}$), and radial diffusivity ($\lambda_{\perp}$) in the optic tracts and internal capsules between glaucoma (*black*) and control groups (*white*). A *t* test between glaucoma and control cats: $^{**}P < 0.01$, $^{****}P < 0.0001$. Data are displayed as box and whisker plots, with caps representing minimum and maximum values, and boxes representing interquartile range with median line shown.

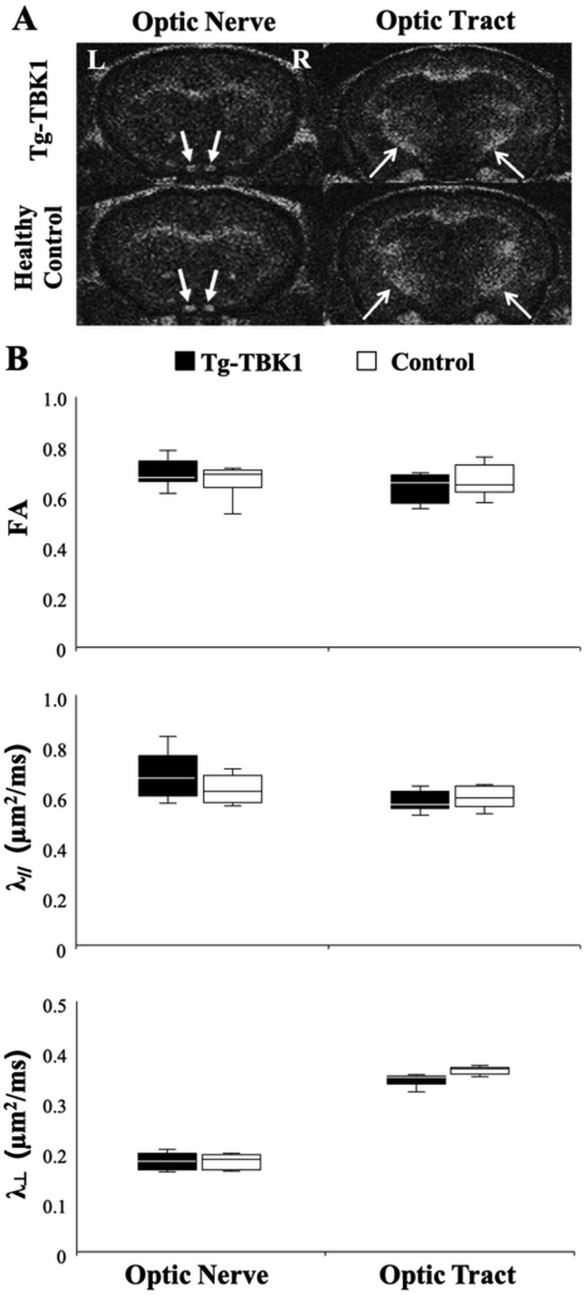

Figure 5. DTI of the optic nerve and optic tract in transgenic *TBK1* (Tg-*TBK1*) mice and age-matched healthy controls. (**A**) FA maps at the level of the optic nerves (*closed arrows*) and optic tracts (*open arrows*) in the Tg-*TBK1* mice (*top row*) and age-matched controls (*bottom row*). (**B**) Comparisons of FA, axial diffusivity ($\lambda_{//}$), and radial diffusivity ($\lambda_{\perp}$) between Tg-*TBK1* mice and age-matched controls revealed no apparent difference in either the optic nerves or optic tracts (*t* tests, $P > 0.05$). Data are displayed as box and whisker plots, with caps representing minimum and maximum values, and boxes representing interquartile range with median line shown.

of destruction in the optic nerve and optic tract than the other one.

Compared with chronic experimental glaucoma, models using more acute insults to the retina and optic nerve have been shown to produce different DTI manifestations. For instance, traumatic optic neuropathy by optic nerve crush, *N*-methyl-D-aspartate–induced excitotoxic retinal injury,[55,56] and retinal ischemia–reperfusion injury secondary to transiently elevated IOP at 100 to 120 mm Hg for 65 minutes can lead to initial decreases in FA and $\lambda_{//}$ before an $\lambda_{\perp}$ increase along the visual pathway. These findings suggest that acute and chronic insults in the eye and optic nerve axons may involve different pathophysiological

Investigative Ophthalmology & Visual Science

events that are detectable by examining their DTI characteristics. Also, chronic experimental and spontaneous glaucoma may involve a complex interplay of neurodegenerative processes beyond the early axonal and delayed myelin injuries suggested in the acute models.

Although the transgenic *TBK1* mice displayed no apparent DTI change along with normal IOP, it is important to note that the *TBK1* mice show only a modest 13% RGC loss at 18 months.[23] In comparison, the *LTBP2* mutant cats and DBA/2J mice show greater decreases in the RGC of 64% and 44%, respectively, in the later disease stages.[22,23,28,57] In addition, although neuroinflammation, including microglial proliferation and activation, has been identified in the other glaucoma animal models studied here,[47–49,58–60] no evidence of neuroinflammation has been reported in the transgenic hemizygous *TBK1* mice used in our study. Further studies may include analysis of mice that have more copies of *TBK1* transgene incorporated in their genome, the *Optineurin E50K* mutant,[61,62] as well as concurrent *TBK1* and *E50K* interactions,[57] to determine their contributions to disease severity and to characterize the neuropathophysiology of normotensive glaucoma. Future DTI studies may also determine the extent of visual pathway changes in both ocular hypertensive and normotensive glaucoma animal models with respect to different genetic backgrounds, IOP exposure, age, and so on.[63,64,83,84]

There are inherent limitations to this study and to the animal models used. Although DTI changes were consistently observed in the optic nerve of the rodent models of chronic IOP elevation, only the DBA/2J mouse model demonstrated DTI changes in the optic tract at the later time point. Future longitudinal studies at different stages of the glaucoma effect could provide greater insight into the spatiotemporal sequence of disease progression in these models. Additionally, future work should consider correlations of DTI changes in the optic nerve axons with individual IOPs as well as structural and functional damage in the eye and neural pathway via optical coherence tomography and electrophysiology. Histologic confirmations will also be useful in the future to address the origins of FA, $\lambda_{//}$, and $\lambda_{\perp}$ changes observed in our glaucoma animal models relative to the extents of neurodegenerative processes such as axonal injury, demyelination, inflammation, and glial activation at each experimental time point.[40,46–51] One limitation inherent to rodent models is that, although human glaucoma is associated with structural changes at the level of the lamina cribrosa, rodents lack this structure and only possess the glial lamina. Despite such limitations, the rodent models remain useful for testing pathophysiological mechanisms independent of the lamina cribrosa,[15,16,65] the genetic contributions to glaucomatous damages, as well as novel neurotherapeutics options for glaucoma,[66–68] given their wide availability for genetic modifications, and the relatively low cost compared with feline and nonhuman primate models. In contrast, the feline optic nerve head possesses a robust lamina cribrosa with microarchitecture and cell population that closely resembles humans.[69] However, only a limited number of cats were available for imaging at the time of experiments. Future studies may use DTI in larger samples of glaucoma animal models in higher order species to examine how the visual system alters trans-synaptically over time.[70,71]

In summary, the present study showed that chronic IOP elevation was accompanied by decreased FA and increased $\lambda_{\perp}$ along the optic nerve or optic tract, suggestive of disrupted microstructural integrity in both inducible and genetic glaucoma animal models. The association of elevated IOP in different models matched with signs of degeneration along the visual pathway, which supported the notion that these animal models were valid surrogates of glaucoma. The effects on $\lambda_{//}$ varied between models, indicative of the inter-model differences and the complex interplay between etiology, severity of damage, and stage of pathological change. This imaging work characterized the structural damage in various commonly used animal models of glaucoma and demonstrated the utility of DTI as a noninvasive tool for deciphering the structural pathobiology of glaucoma. The findings presented here may contribute to a better understanding of the neurologic features of each of the animal models, which can then be used to design more informed glaucoma basic research studies using noninvasive diffusion-weighted imaging modalities. Apart from DTI, higher order diffusion imaging modalities, such as diffusion basis spectrum imaging,[72–74] and the extended diffusion kurtosis imaging model called white matter tract integrity model[41,75] can be combined with DTI to differentiate between intra-axonal and extra-axonal microenvironments and a provide more accurate characterization of the tissue architecture.[76,77] Future studies are warranted that examine how these diffusion imaging modalities, in addition to other multiparametric MRI techniques,[76,78–82] may be useful tools to complement direct ophthalmoscopy in studying the pathophysiology underlying glaucomatous neurodegeneration, defining the microstructural disruption resulting from glaucoma, and monitoring disease progression and treatment response noninvasively along the visual pathway.

Acknowledgments

The authors thank Alex Shimony, Kenneth Waller, and Pouria Mossahebi at the University of Wisconsin-Madison for their technical support.

Supported in part by the National Institutes of Health R01-EY028125, R01-EY025643, K08EY018609, P30EY0016665, and UL1TR000427 (Bethesda, Maryland); BrightFocus Foundation G2013077, G2016030, and G2019103 (Clarksburg, Maryland); Feldstein Medical Foundation (Clifton, New Jersey); Research to Prevent Blindness/Stavros Niarchos Foundation International Research Collaborators Award (New York, New York); and unrestricted funds from Research to Prevent Blindness (New York, New York) to NYU Langone Health Department of Ophthalmology and the Department of Ophthalmology and Visual Sciences at University of Wisconsin-Madison.

Disclosure: **M.K. Colbert**, None; **L.C. Ho**, None; **Y. van der Merwe**, None; **X. Yang**, None; **G.J. McLellan**, None; **S.A. Hurley**, None; **A.S. Field**, None; **H. Yun**, None; **Y. Du**, None; **I.P. Conner**, None; **C. Parra**, None; **M.A. Faiq**, None; **J.H. Fingert**, None; **G. Wollstein**, None; **J.S. Schuman**, None; **K.C. Chan**, None

References

1. Quigley HA, Broman AT. The number of people with glaucoma worldwide in 2010 and 2020. *Br J Ophthalmol*. 2006;90:262–267.
2. Dandona L, Dandona R. What is the global burden of visual impairment? *BMC Med*. 2006;4:6.
3. Tham YC, Li X, Wong TY, Quigley HA, Aung T, Cheng CY. Global prevalence of glaucoma and projections of glaucoma

burden through 2040: a systematic review and meta-analysis. *Ophthalmology*. 2014;121:2081–2090.
4. Leske MC, Heijl A, Hyman L, Bengtsson B, Komaroff E. Factors for progression and glaucoma treatment: the Early Manifest Glaucoma Trial. *Curr Opin Ophthalmol*. 2004;15:102–106.
5. Susanna R, De Moraes CG, Cioffi GA, Ritch R. Why so people (still) go blind from glaucoma? *Transl Vis Sci Technol*. 2015;4:1.
6. Gordon MO, Beiser JA, Brandt JD, et al. The Ocular Hypertension Treatment Study: baseline factors that predict the onset of primary open-angle glaucoma. *Arch Ophthalmol*. 2002;120:714–720; discussion 829-730.
7. Crish SD, Sappington RM, Inman DM, Horner PJ, Calkins DJ. Distal axonopathy with structural persistence in glaucomatous neurodegeneration. *Proc Natl Acad Sci USA*. 2010;107:5196–5201.
8. Calkins DJ, Horner PJ. The cell and molecular biology of glaucoma: axonopathy and the brain. *Invest Ophthalmol Vis Sci*. 2012;53:2482–2484.
9. Sponsel WE, Groth SL, Satsangi N, Maddess T, Reilly MA. Refined data analysis provides clinical evidence for central nervous system control of chronic glaucomatous neurodegeneration. *Transl Vis Sci Technol*. 2014;3:1.
10. Reilly MA, Villarreal A, Maddess T, Sponsel WE. Refined frequency doubling perimetry analysis reaffirms central nervous system control of chronic glaucomatous neurodegeneration. *Transl Vis Sci Technol*. 2015;4:7.
11. Sponsel WE, Johnson SL, Trevino R, et al. Pattern electroretinography and visual evoked potentials provide clinical evidence of CNS modulation of high- and low-contrast VEP latency in glaucoma. *Transl Vis Sci Technol*. 2017;6:6.
12. Yucel YH, Zhang Q, Gupta N, Kaufman PL, Weinreb RN. Loss of neurons in magnocellular and parvocellular layers of the lateral geniculate nucleus in glaucoma. *Arch Ophthalmol*. 2000;118:378–384.
13. Kasi A, Faiq MA, Chan KC. *in vivo* imaging of structural, metabolic and functional brain changes in glaucoma. *Neural Regen Res*. 2019;14:446–449.
14. Yucel YH, Zhang Q, Weinreb RN, Kaufman PL, Gupta N. Effects of retinal ganglion cell loss on magno-, parvo-, koniocellular pathways in the lateral geniculate nucleus and visual cortex in glaucoma. *Prog Retin Eye Res*. 2003;22:465–481.
15. Dey A, Manthey AL, Chiu K, Do CW. Methods to induce chronic ocular hypertension: reliable rodent models as a platform for cell transplantation and other therapies. *Cell Transplant*. 2018;27:213–229.
16. Huang W, Hu F, Wang M, et al. Comparative analysis of retinal ganglion cell damage in three glaucomatous rat models. *Exp Eye Res*. 2018;172:112–122.
17. Song SK, Sun SW, Ju WK, Lin SJ, Cross AH, Neufeld AH. Diffusion tensor imaging detects and differentiates axon and myelin degeneration in mouse optic nerve after retinal ischemia. *Neuroimage*. 2003;20:1714–1722.
18. Sun SW, Liang HF, Le TQ, Armstrong RC, Cross AH, Song SK. Differential sensitivity of *in vivo* and ex vivo diffusion tensor imaging to evolving optic nerve injury in mice with retinal ischemia. *Neuroimage*. 2006;32:1195–1204.
19. Zhang X, Sun P, Wang J, Wang Q, Song SK. Diffusion tensor imaging detects retinal ganglion cell axon damage in the mouse model of optic nerve crush. *Invest Ophthalmol Vis Sci*. 2011;52:7001–7006.
20. Xie M, Wang Q, Wu TH, Song SK, Sun SW. Delayed axonal degeneration in slow Wallerian degeneration mutant mice detected using diffusion tensor imaging. *Neuroscience*. 2011;197:339–347.
21. Yun H, Lathrop KL, Yang E, et al. A laser-induced mouse model with long-term intraocular pressure elevation. *PLoS One*. 2014;9:e107446.
22. Kuehn MH, Lipsett KA, Menotti-Raymond M, et al. A mutation in LTBP2 causes congenital glaucoma in domestic cats (Felis catus). *PLoS One*. 2016;11:e0154412.
23. Fingert JH, Miller K, Hedberg-Buenz A, et al. Transgenic TBK1 mice have features of normal tension glaucoma. *Hum Mol Genet*. 2017;26:124–132.
24. Chen H, Wei X, Cho KS, et al. Optic neuropathy due to microbead-induced elevated intraocular pressure in the mouse. *Invest Ophthalmol Vis Sci*. 2011;52:36–44.
25. Sappington RM, Carlson BJ, Crish SD, Calkins DJ. The microbead occlusion model: a paradigm for induced ocular hypertension in rats and mice. *Invest Ophthalmol Vis Sci*. 2010;51:207–216.
26. John SW, Smith RS, Savinova OV, et al. Essential iris atrophy, pigment dispersion, and glaucoma in DBA/2J mice. *Invest Ophthalmol Vis Sci*. 1998;39:951–962.
27. Libby RT, Anderson MG, Pang IH, et al. Inherited glaucoma in DBA/2J mice: pertinent disease features for studying the neurodegeneration. *Vis Neurosci*. 2005;22:637–648.
28. Hirt J, Porter K, Dixon A, McKinnon S, Liton PB. Contribution of autophagy to ocular hypertension and neurodegeneration in the DBA/2J spontaneous glaucoma mouse model. *Cell Death Discov*. 2018;4:14.
29. Danias J, Lee KC, Zamora MF, et al. Quantitative analysis of retinal ganglion cell (RGC) loss in aging DBA/2NNia glaucomatous mice: comparison with RGC loss in aging C57/BL6 mice. *Invest Ophthalmol Vis Sci*. 2003;44:5151–5162.
30. Lu P, Shi L, Du H, et al. Reduced white matter integrity in primary open-angle glaucoma: a DTI study using tract-based spatial statistics. *J Neuroradiol*. 2013;40:89–93.
31. Sidek S, Ramli N, Rahmat K, Ramli NM, Abdulrahman F, Tan LK. Glaucoma severity affects diffusion tensor imaging (DTI) parameters of the optic nerve and optic radiation. *Eur J Radiol*. 2014;83:1437–1441.
32. Murphy MC, Conner IP, Teng CY, et al. Retinal structures and visual cortex activity are impaired prior to clinical vision loss in glaucoma. *Sci Rep*. 2016;6:31464.
33. Schmidt MA, Knott M, Heidemann R, et al. Investigation of lateral geniculate nucleus volume and diffusion tensor imaging in patients with normal tension glaucoma using 7 tesla magnetic resonance imaging. *PLoS One*. 2018;13:e0198830.
34. Xu ZF, Sun JS, Zhang XH, et al. Microstructural visual pathway abnormalities in patients with primary glaucoma: 3 T diffusion kurtosis imaging study. *Clin Radiol*. 2018;73:591e.9–591.e515.
35. Trivedi V, Bang JW, Parra C, et al. Widespread brain reorganization perturbs visuomotor coordination in early glaucoma. *Sci Rep*. 2019;9:14168.
36. Miller N, Liu Y, Krivochenitser R, Rokers B. Linking neural and clinical measures of glaucoma with diffusion magnetic resonance imaging (dMRI). *PLoS One*. 2019;14:e0217011.
37. Wang R, Tang Z, Sun X, et al. White matter abnormalities and correlation with severity in normal tension glaucoma: a whole brain atlas-based diffusion tensor study. *Invest Ophthalmol Vis Sci*. 2018;59:1313–1322.
38. Chang ST, Xu J, Trinkaus K, et al. Optic nerve diffusion tensor imaging parameters and their correlation with optic disc topography and disease severity in adult glaucoma patients and controls. *J Glaucoma*. 2014;23:513–520.
39. Giorgio A, Zhang J, Costantino F, De Stefano N, Frezzotti P. Diffuse brain damage in normal tension glaucoma. *Hum Brain Mapp*. 2018;39:532–541.
40. You Y, Joseph C, Wang C, et al. Demyelination precedes axonal loss in the transneuronal spread of human neurodegenerative disease. *Brain*. 2019;142:426–442.

Investigative Ophthalmology & Visual Science

41. Sun Z, Parra C, Bang JW, et al. Diffusion kurtosis imaging reveals optic tract damage that correlates with clinical severity in glaucoma. *Annu Int Conf IEEE Eng Med Biol Soc*. 2020;2020:1746–1749.
42. Dai H, Yin D, Hu C, et al. Whole-brain voxel-based analysis of diffusion tensor MRI parameters in patients with primary open angle glaucoma and correlation with clinical glaucoma stage. *Neuroradiology*. 2013;55:233–243.
43. Michelson G, Engelhorn T, Warntges S, El Rafei A, Hornegger J, Doerfler A. DTI parameters of axonal integrity and demyelination of the optic radiation correlate with glaucoma indices. *Graefes Arch Clin Exp Ophthalmol*. 2013;251:243–253.
44. Tellouck L, Durieux M, Coupe P, et al. Optic radiations microstructural changes in glaucoma and association with severity: a study using 3Tesla-magnetic resonance diffusion tensor imaging. *Invest Ophthalmol Vis Sci*. 2016;57:6539–6547.
45. Yang Q, Cho KS, Chen H, et al. Microbead-induced ocular hypertensive mouse model for screening and testing of aqueous production suppressants for glaucoma. *Invest Ophthalmol Vis Sci*. 2012;53:3733–3741.
46. Chan KC, Fu QL, Hui ES, So KF, Wu EX. Evaluation of the retina and optic nerve in a rat model of chronic glaucoma using *in vivo* manganese-enhanced magnetic resonance imaging. *Neuroimage*. 2008;40:1166–1174.
47. Wilson GN, Inman DM, Dengler Crish CM, Smith MA, Crish SD. Early pro-inflammatory cytokine elevations in the DBA/2J mouse model of glaucoma. *J Neuroinflammation*. 2015;12:176.
48. Harder JM, Williams PA, Braine CE, et al. Complement peptide C3a receptor 1 promotes optic nerve degeneration in DBA/2J mice. *J Neuroinflammation*. 2020;17:336.
49. Yang X, Hondur G, Tezel G. Antioxidant treatment limits neuroinflammation in experimental glaucoma. *Invest Ophthalmol Vis Sci*. 2016;57:2344–2354.
50. Tezel G, Chauhan BC, LeBlanc RP, Wax MB. Immunohistochemical assessment of the glial mitogen-activated protein kinase activation in glaucoma. *Invest Ophthalmol Vis Sci*. 2003;44:3025–3033.
51. Tezel G, Fourth ARVO/Pfizer Ophthalmics Research Institute Conference Working Group. The role of glia, mitochondria, and the immune system in glaucoma. *Invest Ophthalmol Vis Sci*. 2009;50:1001–1012.
52. Cooper ML, Crish SD, Inman DM, Horner PJ, Calkins DJ. Early astrocyte redistribution in the optic nerve precedes axonopathy in the DBA/2J mouse model of glaucoma. *Exp Eye Res*. 2016;150:22–33.
53. Cooper ML, Collyer JW, Calkins DJ. Astrocyte remodeling without gliosis precedes optic nerve Axonopathy. *Acta Neuropathol Commun*. 2018;6:38.
54. Klistorner A, Vootakuru N, Wang C, et al. Decoding diffusivity in multiple sclerosis: analysis of optic radiation lesional and non-lesional white matter. *PLoS One*. 2015;10:e0122114.
55. Ho LC, Wang B, Conner IP, et al. *in vivo* evaluation of white matter integrity and anterograde transport in visual system after excitotoxic retinal injury with multimodal MRI and OCT. *Invest Ophthalmol Vis Sci*. 2015;56:3788–3800.
56. Kuehn S, Rodust C, Stute G, et al. Concentration-dependent inner retina layer damage and optic nerve degeneration in a NMDA model. *J Mol Neurosci*. 2017;63:283–299.
57. Minegishi Y, Iejima D, Kobayashi H, et al. Enhanced optineurin E50K-TBK1 interaction evokes protein insolubility and initiates familial primary open-angle glaucoma. *Hum Mol Genet*. 2013;22:3559–3567.
58. Suri F, Yazdani S, Elahi E. LTBP2 knockdown and oxidative stress affect glaucoma features including TGFbeta pathways, ECM genes expression and apoptosis in trabecular meshwork cells. *Gene*. 2018;673:70–81.
59. Aihara M, Lindsey JD, Weinreb RN. Experimental mouse ocular hypertension: establishment of the model. *Invest Ophthalmol Vis Sci*. 2003;44:4314–4320.
60. Oikawa K, Ver Hoeve JN, Teixeira LBC, et al. Sub-region-specific optic nerve head glial activation in glaucoma. *Mol Neurobiol*. 2020;57:2620–2638.
61. Fingert JH. Primary open-angle glaucoma genes. *Eye (Lond)*. 2011;25:587–595.
62. Rezaie T, Child A, Hitchings R, et al. Adult-onset primary open-angle glaucoma caused by mutations in optineurin. *Science*. 2002;295:1077–1079.
63. Cone FE, Gelman SE, Son JL, Pease ME, Quigley HA. Differential susceptibility to experimental glaucoma among 3 mouse strains using bead and viscoelastic injection. *Exp Eye Res*. 2010;91:415–424.
64. Cone FE, Steinhart MR, Oglesby EN, Kalesnykas G, Pease ME, Quigley HA. The effects of anesthesia, mouse strain and age on intraocular pressure and an improved murine model of experimental glaucoma. *Exp Eye Res*. 2012;99:27–35.
65. Chan KC, Yu Y, Ng SH, et al. Intracameral injection of a chemically cross-linked hydrogel to study chronic neurodegeneration in glaucoma. *Acta Biomater*. 2019;94:219–231.
66. Howell GR, MacNicoll KH, Braine CE, et al. Combinatorial targeting of early pathways profoundly inhibits neurodegeneration in a mouse model of glaucoma. *Neurobiol Dis*. 2014;71:44–52.
67. Faiq MA, Wollstein G, Schuman JS, Chan KC. Cholinergic nervous system and glaucoma: From basic science to clinical applications. *Prog Retin Eye Res*. 2019;72:100767.
68. Williams PA, Harder JM, Foxworth NE, et al. Vitamin B3 modulates mitochondrial vulnerability and prevents glaucoma in aged mice. *Science*. 2017;355:756–760.
69. Oikawa K, Teixeira LBC, Keikhosravi A, Eliceiri KW, McLellan GJ. Microstructure and resident cell-types of the feline optic nerve head resemble that of humans. *Exp Eye Res*. 2021;202:108315.
70. Yan Y, Li L, Preuss TM, Hu X, Herndon JG, Zhang X. *in vivo* evaluation of optic nerve aging in adult rhesus monkey by diffusion tensor imaging. *Quant Imaging Med Surg*. 2014;4:43–49.
71. Wang B, Tran H, Smith MA, et al. In-vivo effects of intraocular and intracranial pressures on the lamina cribrosa microstructure. *PLoS One*. 2017;12:e0188302.
72. Kim JW, Andersson JL, Seifert AC, et al. Incorporating nonlinear alignment and multi-compartmental modeling for improved human optic nerve diffusion imaging. *Neuroimage*. 2019;196:102–113.
73. Wang Y, Wang Q, Haldar JP, et al. Quantification of increased cellularity during inflammatory demyelination. *Brain*. 2011;134:3590–3601.
74. Wang X, Cusick MF, Wang Y, et al. Diffusion basis spectrum imaging detects and distinguishes coexisting subclinical inflammation, demyelination and axonal injury in experimental autoimmune encephalomyelitis mice. *NMR Biomed*. 2014;27:843–852.
75. Fieremans E, Jensen JH, Helpern JA. White matter characterization with diffusional kurtosis imaging. *Neuroimage*. 2011;58:177–188.
76. Li T, Qu X, Chen W, et al. Altered information flow and microstructure abnormalities of visual cortex in normal-tension glaucoma: evidence from resting-state fMRI and DKI. *Brain Res*. 2020;1741:146874.
77. Nucci C, Garaci F, Altobelli S, et al. Diffusional kurtosis imaging of white matter degeneration in glaucoma. *J Clin Med*. 2020;9:3122.

Investigative Ophthalmology & Visual Science

78. Chan KC, So KF, Wu EX. Proton magnetic resonance spectroscopy revealed choline reduction in the visual cortex in an experimental model of chronic glaucoma. *Exp Eye Res*. 2009;88:65–70.
79. Deng W, Faiq MA, Liu C, Adi V, Chan KC. Applications of Manganese-enhanced magnetic resonance imaging in ophthalmology and visual neuroscience. *Front Neural Circuits*. 2019;13:35.
80. Deng W, Liu C, Parra C, et al. Quantitative imaging of the clearance systems in the eye and the brain. *Quant Imaging Med Surg*. 2020;10:1–14.
81. Yang XL, van der Merwe Y, Sims J, et al. Age-related changes in eye, brain and visuomotor behavior in the DBA/2J mouse model of chronic glaucoma. *Sci Rep*. 2018;8:4643.
82. Voorhees AP, Ho LC, Jan NJ, et al. Whole-globe biomechanics using high-field MRI. *Exp Eye Res*. 2017;160:85–95.
83. van der Merwe Y, Murphy MC, Sims JR, et al. Citicoline modulates glaucomatous neurodegeneration through intraocular pressure-independent control. *Neurotherapeutics*. 2021;1–21.
84. Zhu J, Sainulabdeen A, Akers K, et al. Oral scutellarin treatment ameliorates retinal thinning and visual deficits in experimental glaucoma. *Front Med*. 2021;8:681169.